Analysis and Elimination of Hysteresis and Noisy Precursors in Power Amplifiers

Sanggeun Jeon, *Student Member, IEEE*, Almudena Suárez, *Senior Member, IEEE*, and David B. Rutledge, *Fellow, IEEE*

***Abstract*—Power amplifiers (PAs) often exhibit instabilities leading to frequency division by two or oscillations at incommensurate frequencies. This undesired behavior can be detected through a large-signal stability analysis of the solution. However, other commonly observed phenomena are still difficult to predict and eliminate. In this paper, the anomalous behavior observed in a Class-E PA is analyzed in detail. It involves hysteresis in the power-transfer curve, oscillation, and noisy precursors. The precursors are pronounced bumps in the power spectrum due to noise amplification under a small stability margin. The correction of the amplifier performance has required the development of a new technique for the elimination of the hysteresis. Instead of a trial-and-error procedure, this technique, of general application to circuit design, makes use of bifurcation concepts to suppress the hysteresis phenomenon through a single simulation on harmonic-balance software. Another objective has been the investigation of the circuit characteristics that make the noisy precursors observable in practical circuits and a technique has been derived for their elimination from the amplifier output spectrum. All the different techniques have been experimentally validated.**

***Index Terms*—Bifurcation, class-E amplifier, hysteresis, noisy precursor, stability, synchronization.**

I. Introduction

POWER amplifiers (PAs) often exhibit unstable behavior from a certain level of the input power [1]–[4]. Frequency divisions by two and oscillations at incommensurate frequencies can be predicted through a large-signal stability analysis of the amplifier solution [4]–[7]. In a previous work by the authors [4], techniques were also presented for the efficient determination, through bifurcation detection, of the circuit parameters giving unstable behavior. Oscillatory and chaotic solutions were analyzed in detail, which enabled the derivation of a suitable stabilization technique. However, other phenomena, whose origins are difficult to identify, are also commonly observed in the measurement of PAs. This study has been motivated by the anomalous behavior of a Class-E PA [8]. In the intermediate input-power range, this circuit exhibited pronounced noise bumps at frequencies different from the input-drive frequency, which degraded the amplifier performance. The bumps were observable for a relatively large input-power interval until an oscillation was suddenly obtained. The frequency of this oscillation f_a mixed with the input-drive frequency $f_{\rm in}$ to give rise to sidebands whose frequencies were surprisingly different from the central frequencies of the previous noise bumps.

As will be shown, the observed phenomenon involves hysteresis in the power-transfer curve and sideband noise amplification [9], the latter giving rise to the spectrum bumps, also called noisy precursors [10]. These undesired phenomena may also be obtained in PAs for communications in which linearity and spectral purity are essential. The hysteresis causes sudden spectral growth and disrupts the linearity of amplifiers. The noisy precursors degrade the spectral purity and, particularly, bumps around the input-drive frequency may give rise to interference with other channels.

The in-depth investigation of the undesired behavior of PAs requires the combination of different analysis techniques, some of which will be presented here for the first time. The hysteresis in the $P_{\rm in} - P_{\rm out}$ curve is due to the existence of a multivalued section in the solution curve traced versus $P_{\rm in}$ as a result of infinite-slope points or turning points [11], [12] occurring in this curve. When using harmonic balance (HB), the multivalued solution curve can be traced by means of a suitable continuation technique, like the switching-parameter algorithm [11]–[13]. Here, a technique will be presented to obtain the multivalued curve in commercial HB software, unable to pass through the tuning points. However, the actual goal of the designer is the suppression of the hysteresis phenomenon, which is generally carried out through a trial-and-error procedure. In order to improve the design efficiency, a new technique is proposed here allowing the removal of the turning points through a single simulation on commercial HB. It relies on the tracing of a turning-point locus on the plane defined by the input power and a suitable stabilization parameter.

As already discussed, high-power bumps were observed in the output power spectrum of the Class-E PA. In previous studies, these bumps have been related to noise amplification coming from a small stability margin [9]. The circuit resonant frequencies have low damping and, under the continuous noise perturbations, give rise to bumps in the output power spectrum. If a circuit parameter, such as the input power, is varied and the near-critical poles approach the imaginary axis, the noise bumps become narrower and higher. If the poles cross the imaginary axis, a bifurcation occurs and, from this parameter value, the bumps become distinct spectral lines. One of the objectives of this study is the study of this phenomenon in PAs.

The continuous pole displacement, approaching the imaginary axis, takes place in any circuit evolving to an unstable regime. However, the noisy precursors are not always observable. Another aspect that will be investigated here is the reason for the observation of this phenomenon in particular circuits only. Pole-zero identification [6], [7] will be applied to follow

Manuscript received June 20, 2005; revised October 14, 2005. This work was supported by the Lee Center for Advanced Networking, California Institute of Technology and by Qualcomm.

S. Jeon and D. B. Rutledge are with the Department of Electrical Engineering, California Institute of Technology, Pasadena, CA 91125 USA (e-mail: sjeon@caltech.edu; rutledge@caltech.edu).

A. Suárez is with the Communications Engineering Department, University of Cantabria, 39005 Santander, Spain (e-mail: suareza@unican.es).

Digital Object Identifier 10.1109/TMTT.2005.864125

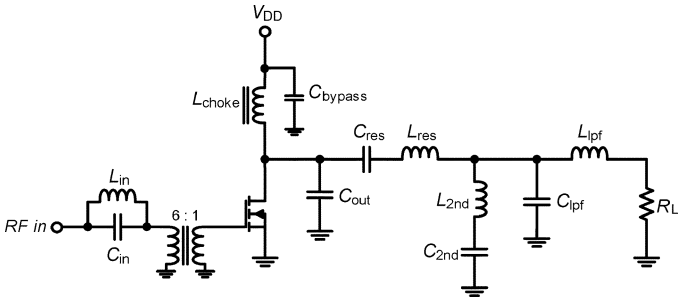

Fig. 1. Schematic of the class-E PA at 7.4 MHz [8].

the evolution of the system poles, which will be related to the noise amplification. The output noise spectrum will be simulated with both the conversion-matrix approach [14] and the envelope transient [15], [16]. The latter enables a prediction of nonlinear phenomena occurring for high-power bumps or in the immediate neighborhood of the bifurcation. A technique will also be presented for the elimination of noisy precursors from the amplifier output spectrum.

This paper is organized as follows. In Section II, the measurements of the Class-E PA, with anomalous behavior, are presented. In Section III, the amplifier solution and its stability are analyzed versus the input power. In Section IV, the noisy precursors are simulated with the conversion-matrix approach and the envelope transient. In Section V, a general technique for the elimination of hysteresis in the $P_{\rm in} - P_{\rm out}$ curve of PAs is presented and applied to the Class-E PA. Experimental confirmation is also shown. In Section VI, a technique for the elimination of noisy precursors is presented and applied to the Class-E PA with experimental verification.

II. Experimental Measurements on the Class-E PA

The schematic of the Class-E PA is shown in Fig. 1. The output capacitance $C_{\rm out}$ and a resonant tank composed of $C_{\rm res}$ and $L_{\rm res}$ fulfill the Class-E tuning together with the transistor driven as a switch [17], [18]. The resonant tank is slightly mistuned from the operating frequency $f_{\rm in} = 7.4$ MHz to present a zero-voltage switching characteristic to the drain voltage. In order to suppress the second harmonic level below -40 dBc, a second harmonic trap ($C_{\rm 2nd}$ and $L_{\rm 2nd}$) is used at the output. This also performs the output impedance transformation to 8 Ω, an appropriate load impedance for switching operation. In addition, a low-pass filter ($C_{\rm lpf}$ and $L_{\rm lpf}$) is added to suppress VHF harmonic components from the output spectrum at least 40 dB below the fundamental. The amplifier achieves an output power of 360 W with a gain of 16.1 dB and a drain efficiency of 86.1% at 7.4 MHz, when it is driven with sufficient input power for saturated operation. The input voltage standing-wave ratio (VSWR) is 1.7.

We observe different phenomena in the measurements of the Class-E amplifier. As the input power increases from zero, only leakage output power at the input-drive frequency $f_{\rm in}$ is initially obtained. This is in good agreement with the fact that the transistor in the switching amplifier is not turned on below a certain level of input power. From the input power $P_{\rm in} = 0.5$ W, noise bumps of relatively high power then arise in the spectrum. There are three bumps centered about $f_c = 560$ kHz and $f_{\rm in} \pm f_c$, respectively [see Fig. 2(a)]. As the input power is further increased, f_c decreases and the bumps about $f_{\rm in}$ become closer. The bump power also increases [see Fig. 2(b)] until, at $P_{\rm in} = 0.83$ W, an oscillation is obtained at the frequency $f_a = 1$ MHz [see Fig. 2(c)], which is quite different from f_c. From this power value, the circuit operates in a self-oscillating mixer regime, at the two fundamentals $f_{\rm in}$ and f_a [see Fig. 2(c)]. The high phase noise indicates a low quality factor of the oscillation. The oscillation frequency is close to $f_{\rm in}/7$, which gives rise to spectral lines at short frequency distance from the oscillation harmonics.

At the power value $P_{\rm in} = 0.89$ W, a frequency division by 7 is obtained [see Fig. 2(d)]. The synchronization at $f_a/f_{\rm in} = 1/7$ is maintained for the input-power interval from 0.89 to 0.92 W. The synchronization capability at this high-harmonic order also indicates a low quality factor of the oscillation. When the power level is higher than $P_{\rm in} = 0.92$ W, the circuit behaves again as a self-oscillating mixer. Finally, at $P_{\rm in} = 1.7$ W, the oscillation is extinguished and, from this power value on, the amplifier operates in the desired periodic regime [see Fig. 2(e)]. For reasons to be given later, we did not notice hysteresis in these initial measurements. When reducing the input power from power levels above 1.7 W, all the transitions between the different regimes seemed to occur for the same indicated $P_{\rm in}$ values.

As stated in the introduction, the noise bumps are due to noise amplification about the natural frequencies of the circuit when the stability margin is small. Thus, the spectral lines due to the oscillation should be generated at frequencies near $kf_{\rm in} \pm f_c$, with a k integer, which are the central bump frequencies. However, in the Class-E amplifier, there is a substantial difference between the bump frequency f_c and oscillation frequency f_a. To give an explanation of this and other observed phenomena, several analysis techniques will be combined in Section III.

III. Nonlinear Analysis of the Class-E PA

The analysis of the Class-E amplifier will be carried out in three different steps. Initially, its power-transfer curve will be obtained through an HB continuation technique. In a second step, stability-analysis techniques will be applied to study the amplifier stability along the resulting solution curve. Finally, the oscillatory solution will be analyzed using two-tone HB.

A. Analysis of the Power-Transfer Curve

A discontinuity was observed when sweeping the input power, which indicated a possible hysteresis phenomenon. This is caused by turning points or infinite-slope points of the solution curve, at which the Jacobian matrix of the HB system becomes singular [11]. The used commercial HB software is unable to pass through the turning points. To overcome this difficulty, an auxiliary generator (AG), consisting of a voltage source and an ideal bandpass filter [11], is introduced into the circuit. This AG will operate at the input-drive frequency $f_{\rm AG} = f_{\rm in}$ and must not perturb the circuit steady-state solution. This is ensured by imposing a zero value to its current–voltage relationship $Y_{\rm AG} = I_{\rm AG}/V_{\rm AG} = 0$, where $I_{\rm AG}$ and $V_{\rm AG}$ are the current and voltage of the AG, respectively. The equation $Y_{\rm AG} = 0$ is solved through error-minimization or optimization procedures with the HB system as the inner loop. In the curve sections with low slope with respect to the input

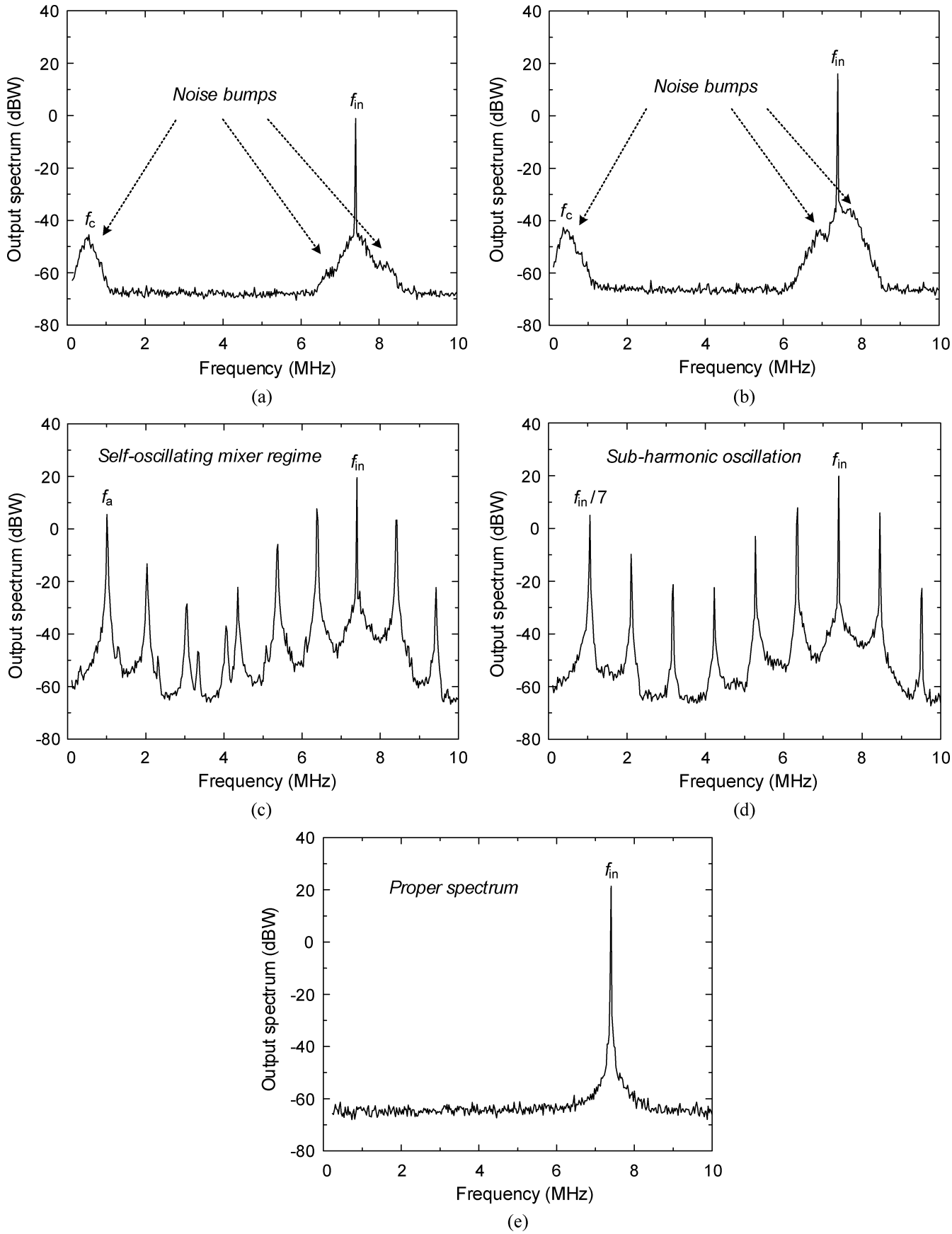

Fig. 2. Measured output power spectrum of the class-E PA for different input power values. Resolution bandwidth = 3 kHz. (a) $P_{\rm in} = 0.5$ W. Pronounced noise bumps are observed about the frequencies $f_c = 560$ kHz and $f_{\rm in} \pm f_c$. (b) $P_{\rm in} = 0.8$ W. The bump frequency f_c is lower and its power is higher. (c) $P_{\rm in} = 0.83$ W. An oscillation suddenly arises at the frequency $f_a = 1$ MHz. (d) $P_{\rm in} = 0.89$ W. Frequency division by 7. The seventh harmonic of the oscillation is synchronized to the input frequency. (e) $P_{\rm in} = 4.0$ W. Proper operation of the amplifier.

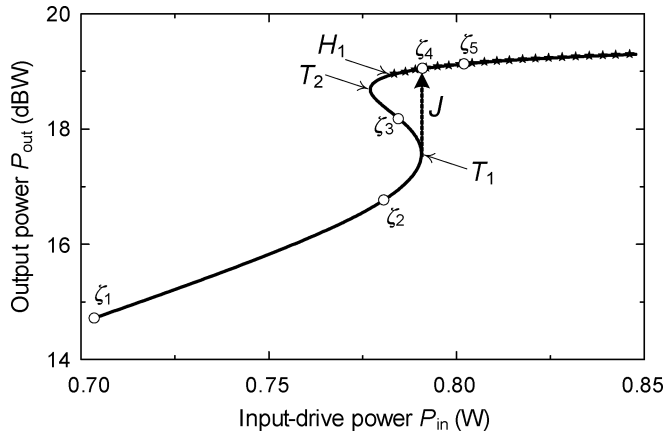

Fig. 3. Multivalued $P_{\rm in} - P_{\rm out}$ curve of the class-E PA, obtained with the AG-based switching-parameter technique. The section in which the amplifier behaves in self-oscillating mixer regime is indicated by stars.

power, this power is used as the sweep parameter and the equation is solved in terms of the AG amplitude $|V_{\rm AG}|$ and its phase $\phi_{\rm AG}$. In the sections with high slope, the sweep parameter is switched to the AG amplitude $|V_{\rm AG}|$ and the equation is solved for $\phi_{\rm AG}$ and $P_{\rm in}$. In the Class-E PA, the AG is connected to the transistor drain terminal. Using the described technique, it has been possible to obtain the multivalued $P_{\rm in} - P_{\rm out}$ curve of Fig. 3.

The next step will be the stability analysis of the amplifier periodic solution along the multivalued curve of Fig. 3, which will be carried out through a sequential application of the pole-zero identification technique [4], [6], [7]. For the Class-E amplifier, a small-signal current source at the frequency f is connected at the transistor drain terminal in order to obtain the required impedance function $Z_{\rm in}(f)$ [6] through the conversion matrix approach. Note that the poles of a periodic solution are nonunivocally defined because adding any integer multiple of $j2\pi f_{\rm in}$ gives another pair of poles with the same real part. These extra poles provide no additional information so only poles between $-j2\pi f_{\rm in}$ and $j2\pi f_{\rm in}$ will be considered here.

Initially, the input power is varied from $P_{\rm in} = 0.70$ W to $P_{\rm in} = 0.79$ W, in a 0.01-W step, following the section $\zeta_1 - \zeta_2 - \zeta_4$ of Fig. 3 with a jump between ζ_2 and ζ_4. The pole-zero identification technique is sequentially applied to each periodic solution obtained with HB. For the calculation of $Z_{\rm in}(f)$, we consider the frequency interval from 1 kHz to 2 MHz. The resulting pole locus is shown in Fig. 4(a), where the two pairs of poles, i.e., $\sigma_1 \pm j2\pi f_1$ and $\sigma_2 \pm j2\pi f_2$, closest to the imaginary axis are represented. The pair $\sigma_1 \pm j2\pi f_1$ is initially much closer to this axis than $\sigma_2 \pm j2\pi f_2$.

As $P_{\rm in}$ increases, both $\sigma_1 \pm j2\pi f_1$ and $\sigma_2 \pm j2\pi f_2$ move rightwards at very different velocity $d\sigma/dP_{\rm in}$. The displacement of $\sigma_2 \pm j2\pi f_2$ is faster than that of $\sigma_1 \pm j2\pi f_1$, which remains in the neighborhood of the axis for all the considered $P_{\rm in}$ values. For $P_{\rm in} = 0.79$ W, due to the jump, there is a discontinuity in the pole locus and an anomalously large shift is obtained in $\sigma_2 \pm j2\pi f_2$, whereas the pair $\sigma_1 \pm j2\pi f_1$ is no longer present. From this power value, the pair $\sigma_2 \pm j2\pi f_2$ is located on the right-hand side of the complex plane. The amplifier periodic solution is unstable, as the pair of poles $\sigma_2 \pm j2\pi f_2$ gives rise to an oscillation at about $f_a = 1$ MHz.

For a detailed study of the pole variations, the sections around the turning points are also analyzed: $\zeta_2 - T_1 - \zeta_3$ and $\zeta_3 - T_2 - H_1 - \zeta_4 - \zeta_5$ of Fig. 3. Note that, unlike the case of Fig. 4(a), $P_{\rm in}$ does not increase monotonically along these sections. The pole-zero identification technique is applied to the solution curve obtained with the AG-based parameter switching technique.

Fig. 4(b) shows the pole evolution along the section $\zeta_2 - T_1 - \zeta_3$. The pair of complex conjugate poles $\sigma_2 \pm j2\pi f_2$ approaches the imaginary axis without crossing it. For clarity, only the evolution of the poles $\sigma_1 \pm j2\pi f_1$ is presented. The considered frequency interval is 0 to 300 kHz. As the input power increases, the two complex conjugate poles remain close to the imaginary axis and from 0.780 to 0.789 W, move nearly vertically, approaching each other, until they meet on the real axis. This gives rise to a qualitative change in the pole configuration, as the two complex conjugate poles become two real ones γ_1 and γ_2 from this power value. By further increasing the power, the two real poles move in opposite directions. The pole γ_1 moves to the right and crosses the imaginary axis at $P_{\rm in} = 0.790$ W. This is the power value at which the turning point T_1 is obtained in the $P_{\rm in} - P_{\rm out}$ curve of Fig. 3, which corresponds with the fact that a pole at zero implies a singularity of the HB Jacobian matrix [11]. From this point, the amplifier periodic solution is unstable.

Fig. 4(c) shows the evolution of the two sets of poles $\sigma_2 \pm j2\pi f_2$ and γ_1, γ_2 along the section $\zeta_3 - T_2 - H_1 - \zeta_4 - \zeta_5$ of the $P_{\rm in} - P_{\rm out}$ curve. The considered frequency interval is 0–1.5 MHz. After passing through zero, γ_1 moves further right, turns, and crosses the imaginary axis through zero again at $P_{\rm in} = 0.777$ W, corresponding to the turning point T_2. The entire section between T_1 and T_2 of the $P_{\rm in} - P_{\rm out}$ curve is unstable because the pole γ_1 is on the right-hand side of the complex plane for the section.

For the same section $\zeta_3 - T_2 - H_1 - \zeta_4 - \zeta_5$ in Fig. 4(c), the poles $\sigma_2 \pm j2\pi f_2$ move to the right, approaching the imaginary axis. At $P_{\rm in} = 0.781$ W, they cross to the right-hand side of the complex plane. A Hopf bifurcation H_1 [11], [19] is obtained, giving rise to an oscillation at about $f_a = 1$ MHz. As $P_{\rm in}$ is further increased, the poles move to the right, turn, and cross again the imaginary axis at $P_{\rm in} = 1.45$ W. At this power value, a Hopf bifurcation H_2 is obtained, which extinguishes the oscillation.

The analysis in Fig. 4 is in correspondence with the measurements of Fig. 2. For the input-power interval 0.5–0.789 W, the first pair of complex conjugate poles $\sigma_1 \pm j2\pi f_1$ is very close to the imaginary axis and the small stability margin explains, as will be shown in Section IV, the observation of the noisy precursors. Actually, the pole frequency f_1 agrees with the bump frequency f_c. As the input power increases, the pole frequency decreases, which explains the decrease of the bump frequency observed in the measurements. At $P_{\rm in} = 0.790$ W, the turning point T_1 is encountered, which ordinarily would give rise to a jump leading to the upper section of the periodic-solution curve. However, this periodic solution is already unstable when the jump takes place because the second pair of complex-conjugate poles $\sigma_2 \pm j2\pi f_2$ with $f_2 = 1$ MHz is on the right-hand side of the complex plane (see the section indicated by stars in Fig. 3). Thus, an oscillation at about $f_a = 1$ MHz is obtained from this power, which is in agreement with the measurement results.

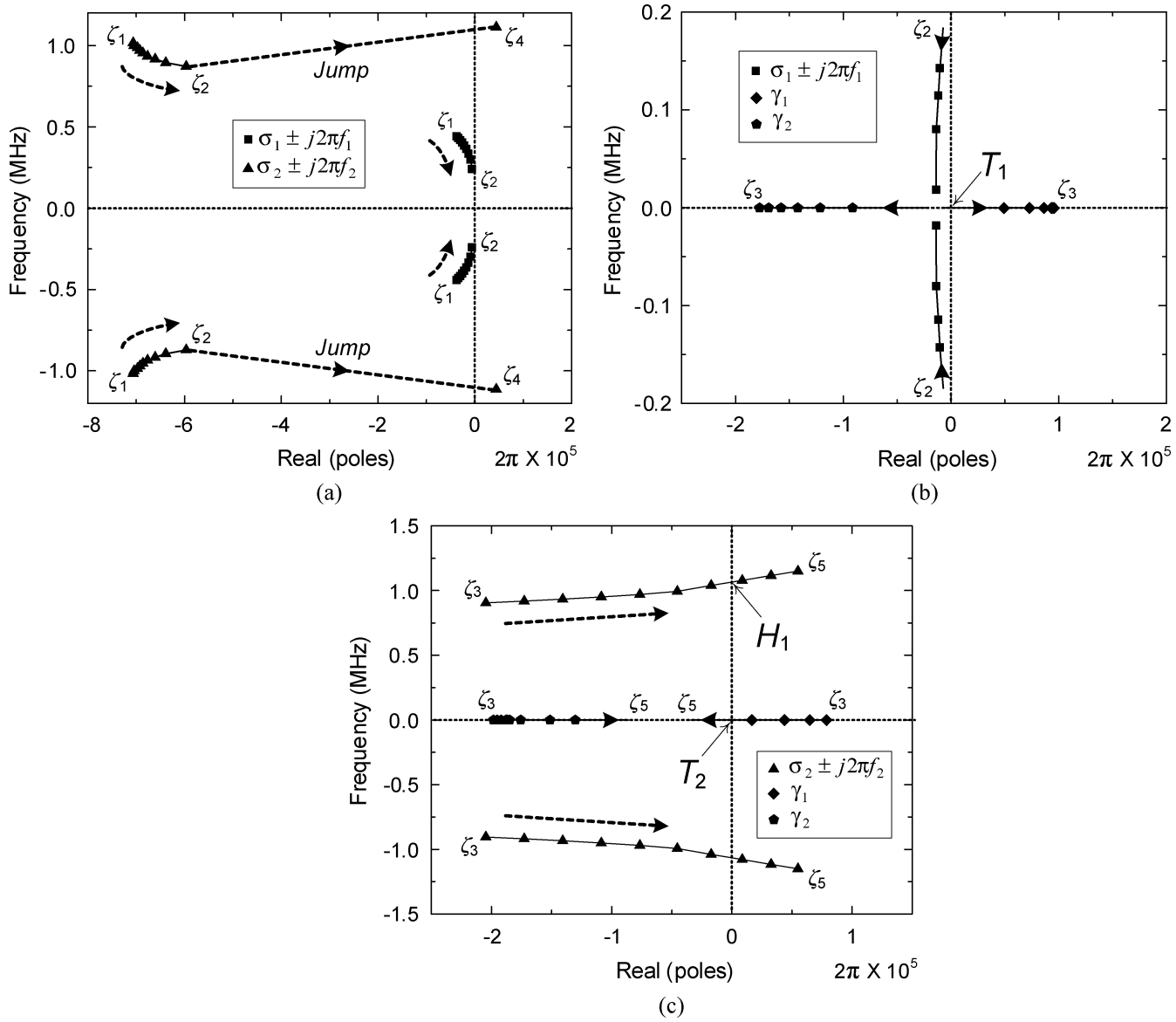

Fig. 4. Pole evolution along the $P_{\rm in} - P_{\rm out}$ curve of Fig. 3. (a) Section $\zeta_1 - \zeta_2 - \zeta_4$ of Fig. 3. The two pairs of poles $\sigma_1 \pm j2\pi f_1$ and $\sigma_2 \pm j2\pi f_2$ closest to the imaginary axis are represented. (b) Section $\zeta_2 - T_1 - \zeta_3$. The complex-conjugate poles $\sigma_1 \pm j2\pi f_1$ approach each other and meet on the real axis. They become two different real poles γ_1 and γ_2 and, from that point, follow opposite directions. One of the real poles crosses the imaginary axis at $P_{\rm in} = 0.790$ W, corresponding to the turning point T_1, and the solution becomes unstable. (c) Section $\zeta_3 - T_2 - H_1 - \zeta_4 - \zeta_5$. The real pole γ_1 crosses the imaginary axis back to the left-hand side at $P_{\rm in} = 0.777$ W, corresponding to the turning point T_2. The pair of complex conjugate poles $\sigma_2 \pm j2\pi f_2$ crosses the imaginary axis to the right-hand side at the Hopf bifurcation H_1, obtained for $P_{\rm in} = 0.781$ W.

In fact, this explains why the hysteresis of Fig. 3 was not initially detected in the measurements. The sudden variation of the output power was attributed solely to the oscillation. In addition, the hysteresis interval was too small to actually observe the difference between the input power values at which the oscillation was generated and extinguished.

B. Analysis of the Oscillatory Solution

For the input-power interval from 0.781 to 1.45 W, the amplifier operates in a self-oscillating mixer regime with the signal at the drive frequency $f_{\rm in}$ mixing with the oscillation at f_a. Using the AG technique [11], it has been possible to obtain the evolution of the oscillatory solution versus the input power, which is represented in Fig. 5(a). Two different curves are traced. One provides the power variation at the oscillation frequency. Increasing the input power, this curve arises at the Hopf bifurcation H_1 and vanishes at the Hopf bifurcation H_2. The second curve provides the output power at the input-drive frequency when the circuit is oscillating. This curve joins the amplifier periodic solution at the two input-power values corresponding to H_1 and H_2. The dashed curve shows the unstable amplifier periodic solution when the circuit is oscillating.

For the considered input frequency $f_{\rm in} = 7.4$ MHz, no harmonic synchronization of the oscillation frequency f_a to the input-drive signal has been observed in simulation, which is attributed to modeling inaccuracies. However, for a somewhat higher frequency $f_{\rm in} = 7.7$ MHz, a frequency division by 7, has been obtained versus $P_{\rm in}$. For the simulation of this divided solution of high order, an AG is connected to the drain terminal in parallel. The AG frequency is determined by the input-drive

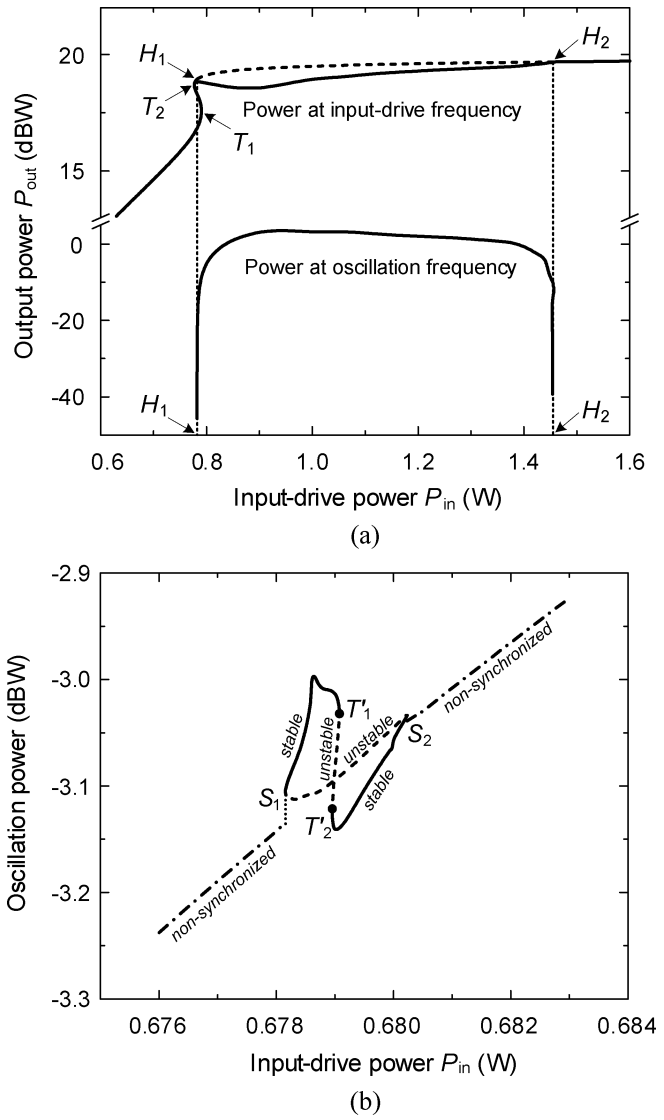

Fig. 5. (a) Bifurcation diagram of the class-E PA versus the input power $P_{\rm in}$. The dashed curve represents the output power of the unstable periodic solution. For the self-oscillating mixer regime, the power variations at both the oscillation frequency and input-drive frequency are represented. The turning points and Hopf bifurcations are also indicated. (b) Synchronization diagram versus $P_{\rm in}$ for frequency division by 7. The closed curve with butterfly shape represents the synchronized solution. This solution is unstable in the dashed-line sections. The power at the oscillation frequency, outside the synchronization region, is also traced.

source and given by $f_{\rm AG} = f_{\rm in}/7$. Instead, the AG phase $\phi_{\rm AG}$ has to be calculated, due to the harmonic relationship between f_a and $f_{\rm in}$ [20].

The application of the above technique to the Class-E amplifier provides the closed curve $S_1 - T'_1 - T'_2 - S_2$ of Fig. 5(b), where the output power at $f_{\rm in}/7$ is represented versus $P_{\rm in}$. The turning points T'_1 and T'_2 give rise to jumps between the different stable sections. The output power at f_a, outside the synchronization range, is also represented. The resulting paths approach the closed curve near the synchronization points S_1 and S_2.

IV. Analysis of Noisy Precursors

Here, a simplified mathematical model is provided for the noisy precursors. The analysis techniques, based on the conversion matrix and envelope transient, will also be discussed. These techniques will be applied in a detailed study of the noise bumps in the Class-E PA.

A. Precursor Model and Analysis Techniques

Let the stable periodic solution $\mathbf{x}_0(t)$ at $f_{\rm in}$ be considered. If a small-amplitude perturbation is applied, an exponential transient will lead back to the original solution $\mathbf{x}_0(t)$. This transient will be dominated by the pole or a pair of complex conjugate poles with the smallest real part, in absolute value [11]. Assuming the dominant poles are $\sigma_c \pm j2\pi f_c$, the smaller the $|\sigma_c|$, the longer the transient at the frequency f_c. Under continuous noise perturbations, bumps will appear in the spectrum about the frequencies $kf_{\rm in} \pm f_c$ [21].

If a parameter η is varied and the near-critical poles $\sigma_c \pm j2\pi f_c$ approach the imaginary axis, the noise bumps will become higher and narrower. If the poles cross the axis, a bifurcation will be obtained, with the bumps turning into distinct spectral lines. Due to this fact, the bumps have been called noisy precursors [9], [10]. The phenomenon can also be explained as a result of negative-resistance parametric amplification [22]. Under the effect of the pumping signal, the nonlinear capacitances will exhibit negative resistance about the circuit resonance frequencies $kf_{\rm in} \pm f_c$. Prior to the bifurcation, the absolute value of this negative resistance will be smaller than the positive resistance exhibited by the embedding circuit. At the bifurcation, the positive resistance equals the negative one. From this point on, the negative resistance will be dominant and the solution will be unstable [23].

Following [9] and [21], it is possible to relate the precursor power with the stability margin and the frequency detuning from the central values $kf_{\rm in} \pm f_c$. Assuming white noise perturbations, the output noise spectrum can be approximately modeled as follows:

$$S(f) \cong \sum_{k=-\infty}^{\infty} \left[\frac{\lambda_k^{lsb}}{\sigma_c^2 + 4\pi^2 (f - kf_{\rm in} + f_c)^2} + \frac{\lambda_k^{usb}}{\sigma_c^2 + 4\pi^2 (f - kf_{\rm in} - f_c)^2} \right] \quad (1)$$

where only the dominant poles $\sigma_c \pm j2\pi f_c + j2\pi k f_{\rm in}$ are taken into account. The coefficients λ_k^{lsb} and λ_k^{usb} depend on the system linearization about the steady-state regime and the input noise sources. There are pairs of Lorentzian lines, centered about the resonance frequencies $kf_{\rm in} \pm f_c$. The height of these lines increases for lower $|\sigma_c|$, which means smaller distance from the critical poles to the imaginary axis. Higher power is also obtained as the frequency approaches the critical values $kf_{\rm in} \pm f_c$. It must also be noted that the linearization becomes invalid in the immediate neighborhood of the bifurcation.

When using HB, the noisy precursors can be analyzed with the conversion matrix approach [14] or the envelope transient [15], [16]. The applicability of the conversion matrix is limited to a relatively low precursor power in order for the linearization about the noiseless solution to be valid. For higher power, the circuit nonlinearities will give rise to gain saturation and other effects [9]. The envelope transient [15], [16] should be used instead, expressing the circuit variables as $\mathbf{x}(t) = \sum_k \mathbf{X}_k(t) e^{j2\pi k f_{\rm in} t}$. Prior to the bifurcation, the time

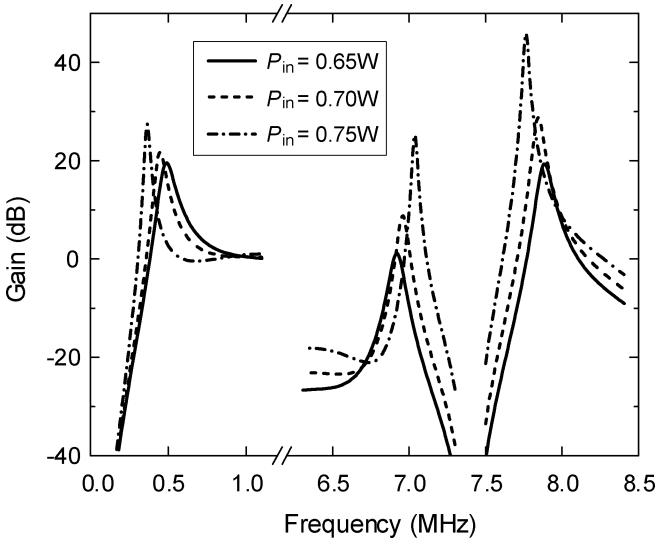

Fig. 6. Validation of sideband amplification. Frequency variation of the current gain from the channel-noise current source to the amplifier output, calculated with the conversion matrix approach. Three different $P_{\rm in}$ values have been considered.

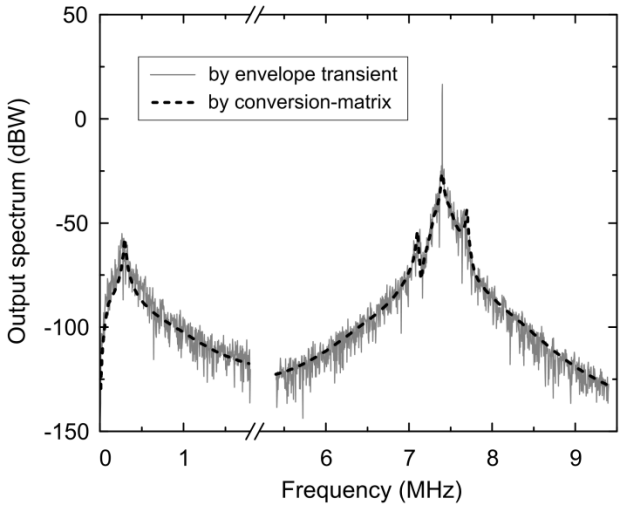

Fig. 7. Analysis of noisy precursors. Comparison of the simulated output spectrum using the conversion-matrix and envelope-transient method. Higher power is obtained at the upper sideband, in agreement with the higher gain value obtained in Fig. 6.

variation $\mathbf{X}_k(t)$ will be exclusively due to the noise perturbations. For the analysis to be accurate, the integration step must be small enough to cover the noisy precursor band about the near-critical frequency f_c. The power spectrum is calculated using a periodogram technique.

B. Application to the Class-E Amplifier

To validate our initial assumption of sideband amplification occurring in this circuit, the conversion-matrix approach will be applied to analyze the gain about the near-critical frequencies f_1, $f_{\rm in}-f_1$, and $f_{\rm in}+f_1$ with f_1 corresponding to the imaginary part of the pair of poles $\sigma_1 \pm j2\pi f_1$ in Fig. 4. The gain from the channel-noise source to the circuit output is initially considered. For this gain analysis, the noise source is replaced with a deterministic current source of small amplitude. Its frequency is swept about f_1, $f_{\rm in}-f_1$, and $f_{\rm in}+f_1$ in three different analyses, calculating the conversion gain at the three considered sidebands.

As a representative case, Fig. 6 shows the gain variation about f_1, $f_{\rm in}-f_1$, and $f_{\rm in}+f_1$ when sweeping the current source about f_1. Three different $P_{\rm in}$ values are considered. Note that the conversion-matrix approach is applied about a different steady-state solution for each $P_{\rm in}$ value. Qualitatively, the gain curves have the Lorentzian shape of (1), except for the asymmetries about the central bump frequencies, which cannot be predicted with this model. The central frequency of the amplification bands changes with $P_{\rm in}$ due to the variation of f_1. Extremely high gains will not be physically observed because small changes in $P_{\rm in}$ cause large gain variations. Furthermore, nonlinear effects occur in the immediate neighborhood of the bifurcation.

For $P_{\rm in} = 0.65$ W, the gain curves are centered about 490 kHz, in agreement with the pole frequency f_1 at this particular power value. The highest gain corresponds to the upper sideband $f_{\rm in}+f$. For the higher power values ($P_{\rm in} = 0.70$ W and $P_{\rm in} = 0.75$ W), the central frequency decreases in good correspondence with the pole displacement of Fig. 4(a) and also with the experimental observations in Fig. 2(a) and (b). The sideband gain increases more rapidly than the lower frequency gain, also in agreement with Fig. 2(a) and (b). Similar qualitative behavior is obtained when sweeping the current source about $f_{\rm in}-f_1$ or $f_{\rm in}+f_1$: the gain increases and bump frequency decreases with the input power, showing the highest gain at the upper sideband. The behavior is also similar when the gain analysis is applied to other noise sources. Note that the purpose of this gain analysis is just to validate our initial assumption of sideband amplification.

For the actual noise analysis, all the different noise sources must be simultaneously considered: the channel noise, the thermal noise from resistive elements, and the noise from the input-drive source, which has been modeled from experimental measurements. The available source providing the necessary power for the switching operation of the amplifier has high noise and constitutes the largest noise contribution. The results obtained with both the conversion-matrix approach and envelope transient are compared in Fig. 7. The good agreement indicates that no relevant nonlinear effects are taking place in the system for this operation condition. The power of the upper sideband about $f_{\rm in}$ is higher than that of the lower sideband, which corresponds with the gain analysis of Fig. 6 and the measurements. As has been verified in simulation, noisy precursors of lower power are still obtained when using an input-drive source of higher spectral purity.

The Class-E amplifier combines two characteristics that contribute to the practical observation of the precursors. The near-critical poles have small derivative $|d\sigma/dP_{\rm in}|$ so they remain close to the imaginary axis for a relatively large $P_{\rm in}$ interval. Also, the gain from the noise sources to the circuit output is high, as shown in Fig. 6. This gain is critical in allowing the precursors to be observed. For other amplifiers operating close to instability, the gain is usually too low and the precursors are below the noise floor of the measurement system.

V. Elimination of the Hysteresis in the $P_{\rm in} - P_{\rm out}$ Curve

As already discussed, the hysteresis is due to the existence of turning points in the $P_{\rm in} - P_{\rm out}$ curve. Thus, the hysteresis can be suppressed if we remove these turning points. Taking the curve in Fig. 3 as an example, the two turning points occur at $P_{\rm in} = 0.790$ W and 0.777 W with a difference of 0.013 W. These points can be removed by making them approach each other and eventually meet in a single point, corresponding to a "cusp" bifurcation through the variation of a suitable circuit parameter μ. This parameter can be either an existing circuit component or an added one for the hysteresis elimination. At the "cusp" bifurcation [19], [24], the two turning points meet and, for a further variation of the parameter, disappear from the solution curve, due to the continuity of the system. This continuity also ensures a limited disturbance of the original amplifier response.

As already stated, the Jacobian matrix of the HB system becomes singular at the turning points due to the existence of a real pole at zero $\gamma = 0$. In [11], it was shown that the Jacobian matrix associated to the nonperturbation equation $Y_{\rm AG} = 0$ also becomes singular at these points. When simulating the amplifier periodic solution, this Jacobian matrix is given by

$$[JY_{\rm AG}] = \begin{bmatrix} \dfrac{\partial Y^r_{\rm AG}}{\partial |V_{\rm AG}|} & \dfrac{\partial Y^r_{\rm AG}}{\partial \phi_{\rm AG}} \\ \dfrac{\partial Y^i_{\rm AG}}{\partial |V_{\rm AG}|} & \dfrac{\partial Y^i_{\rm AG}}{\partial \phi_{\rm AG}} \end{bmatrix} \tag{2}$$

where $Y^r_{\rm AG}$ and $Y^i_{\rm AG}$ are the real and imaginary parts of $Y_{\rm AG}$, respectively. The derivatives are calculated through finite differences using HB.

The cusp point is a co-dimensional 2 bifurcation, requiring the fine tuning of two parameters [19]. One parameter will be $P_{\rm in}$ and the other, the stabilization element μ. In the plane defined by these two parameters, the locus of turning points is given by

$$\begin{aligned} Y_{\rm AG}\big(|V_{\rm AG}|, \phi_{\rm AG}, \mu, P_{\rm in}\big) &= 0 \\ \det\Big[JY_{\rm AG}\big(|V_{\rm AG}|, \phi_{\rm AG}, \mu, P_{\rm in}\big)\Big] &= 0. \end{aligned} \tag{3}$$

The above system contains four real unknowns in three real equations, so a curve is obtained in the plane $(\mu, P_{\rm in})$. All the points in this curve have a real pole at zero $\gamma = 0$.

The curve defined by (3) will be traced from the initial value $\mu = \mu_0$ corresponding to the original circuit. In the case of a multivalued curve like the one in Fig. 3, for $\mu = \mu_0$, there will be two different turning points. Provided there is enough sensitivity to μ, the two turning points will vary versus μ and, at given $\mu = \mu_{\rm cp}$, they will meet in a cusp point, obtained for the input power $P_{\rm in\_cp}$. At the cusp point, the two following conditions are satisfied for the real pole γ:

$$\begin{aligned} \gamma\big(\mu_{\rm cp}, P_{\rm in\_cp}\big) &= 0 \\ \frac{\partial \gamma}{\partial P_{\rm in}}\big(\mu_{\rm cp}, P_{\rm in\_cp}\big) &= 0. \end{aligned} \tag{4}$$

Note that all the rest of turning points, composing the locus defined by (3), fulfill $\partial\gamma/\partial P_{\rm in} \neq 0$, as they give rise to a qualitative stability change in the solution curve. The second condition in (4) comes from the fact that the unstable section between the turning points does not exist any more due to the merging of these points so the real pole does not cross the imaginary axis. Instead, it is tangent to this axis at the origin. For a further μ variation (in the same sense), the solution curve will exhibit no turning points and the hysteresis will be eliminated.

We can implement this technique on a commercial HB simulator. It requires the consideration of the original circuit, plus two identical copies. An AG will be connected to each of the three circuits, with different values of the AG amplitude and phase in each of them. The two copies will enable the calculation of the derivatives that compose the Jacobian matrix (2). The first of the three circuits operates at the nominal values $|V_{\rm AG}|$ and $\phi_{\rm AG}$ and must fulfill the conditions (3). One of the copies operates at $|V_{\rm AG}| + \Delta|V_{\rm AG}|$ and $\phi_{\rm AG}$, and is used for the calculation of the derivative $\partial Y_{\rm AG}/\partial|V_{\rm AG}|$. The other copy operates at $|V_{\rm AG}|$ and $\phi_{\rm AG} + \Delta\phi_{\rm AG}$, and is used for the calculation of the derivative $\partial Y_{\rm AG}/\partial\phi_{\rm AG}$. The three circuits are solved simultaneously in a single HB simulation. In order to obtain the turning-point locus in the single simulation, the phase $\phi_{\rm AG}$ is swept, optimizing $|V_{\rm AG}|$, $P_{\rm in}$, and μ in the nominal circuit in order to fulfill the conditions (3).

After inspection of the Class-E amplifier schematic, it was considered that the variation of the elements in the output low-pass filter, composed of $L_{\rm lpf}$ and $C_{\rm lpf}$, should not strongly affect the drain efficiency and output power. Their possible influence on the turning points of the $P_{\rm in} - P_{\rm out}$ curve was examined. The capacitance $C_{\rm lpf}$ was taken as a stabilization parameter $\mu = C_{\rm lpf}$. The turning-point locus fulfilling (3) was traced in the plane defined by $C_{\rm lpf}$ and $P_{\rm in}$ for three different $L_{\rm lpf}$ values.

The results are shown in Fig. 8. The two $P_{\rm in}$ values obtained for each $L_{\rm lpf}$ and $C_{\rm lpf}$ are the ones corresponding to the turning points in the particular $P_{\rm in} - P_{\rm out}$ curve. For the original amplifier, $L_{\rm lpf} = 257$ nH and $C_{\rm lpf} = 100$ pF, the turning points, indicated with dots in Fig. 8, are the same as those in Fig. 3. As can be seen, the range of $C_{\rm lpf}$ values for which the $P_{\rm in} - P_{\rm out}$ curve exhibits turning points decreases with larger $L_{\rm lpf}$. For each $L_{\rm lpf}$ value, as $C_{\rm lpf}$ decreases, the two turning points approach each other until they meet at the cusp point CP. For smaller $C_{\rm lpf}$, no turning points exist so no hysteresis phenomenon should be observed in the circuit.

The results of Fig. 8 have been verified by tracing the $P_{\rm in} - P_{\rm out}$ curves for $L_{\rm lpf} = 257$ nH and different $C_{\rm lpf}$ values between 80 and 100 pF (Fig. 9). For $C_{\rm lpf} = 100$ pF, two turning points are obtained at the power values predicted by the locus of Fig. 8, and a hysteresis phenomenon is observed. For $C_{\rm lpf} = 90$ pF, the two turning points are closer, in agreement with Fig. 8, and a narrower hysteresis interval is obtained. For $C_{\rm lpf} = 85$ pF, the two turning points meet at the cusp point CP_2. For $C_{\rm lpf} = 80$ pF, no hysteresis is observed. The small disturbance of the original $P_{\rm in} - P_{\rm out}$ characteristic by the application of this technique should also be noted. Similarly small disturbance can be expected regardless of the particular circuit. It is due to the continuity of the system, evolving smoothly when the stabilization parameter is varied.

For $C_{\rm lpf} = 80$ pF, with no hysteresis, a wider $P_{\rm in}$ variation has also been considered for pole-zero identification. For low $P_{\rm in}$, there are two pairs of complex-conjugate poles $\sigma_1 \pm j2\pi f_1$ and $\sigma_2 \pm j2\pi f_2$, as in the original circuit. As $P_{\rm in}$ increases, the poles $\sigma_1 \pm j2\pi f_1$ approach each other, merge, and split into two

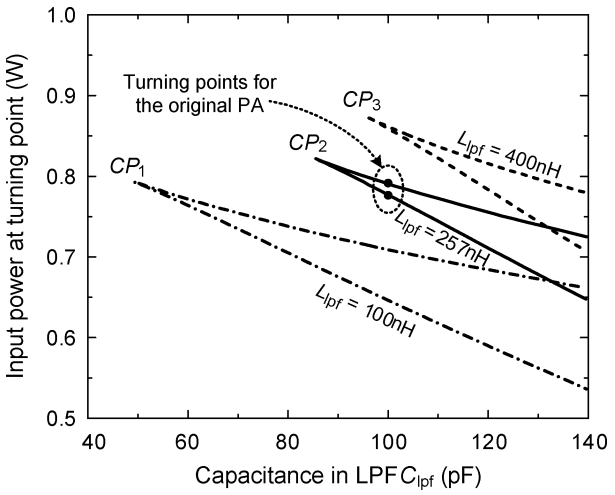

Fig. 8. Locus of turning points in the plane defined by the stabilization parameter $C_{\rm lpf}$ and the input power $P_{\rm in}$. The two power values obtained for each $L_{\rm lpf}$ and $C_{\rm lpf}$ correspond to the two turning points of $P_{\rm in} - P_{\rm out}$ curves, like the ones in Fig. 3. For $C_{\rm lpf}$ smaller than the value corresponding to the cusp point, no turning points are obtained and no hysteresis phenomenon is observed.

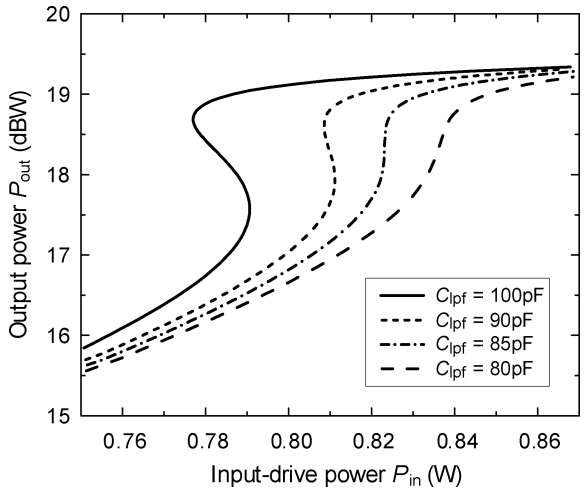

Fig. 9. Elimination of the hysteresis phenomenon with $L_{\rm lpf} = 257$ nH. The hysteresis interval becomes narrower as the capacitance $C_{\rm lpf}$ is reduced, in agreement with the loci in Fig. 8. For capacitor values smaller than $C_{\rm lpf} = 85$ pF, corresponding to the cusp point of this locus, no hysteresis is observed.

real poles at $P_{\rm in} = 0.83$ W that never cross the imaginary axis to the right-hand side. Although the distance of $\sigma_1 \pm j2\pi f_1$ to the imaginary axis has increased, the precursors are still obtained in simulation. On the other hand, for $C_{\rm lpf}$ values below 50 pF, the instability at $f_a = 1$ MHz, due to the pair of complex-conjugate poles $\sigma_2 \pm j2\pi f_2$, is not observed. This is a beneficial effect of the modification of the output low-pass filter. Thus, in order to obtain a $P_{\rm in} - P_{\rm out}$ curve without hysteresis and oscillation, capacitor values below 50 pF must be chosen.

The validity of the new technique has also been experimentally verified. Maintaining $L_{\rm lpf} = 257$ nH, the capacitor value $C_{\rm lpf}$ was changed to below 50 pF. The experimental $P_{\rm in} - P_{\rm out}$ curves of the stabilized amplifier with $C_{\rm lpf} = 20,\ 10,$ and 0 pF are shown in Fig. 10, where they can be compared with the original curve exhibiting a jump. Note that only the curves without oscillation are presented for the stabilized PA. The oscillation

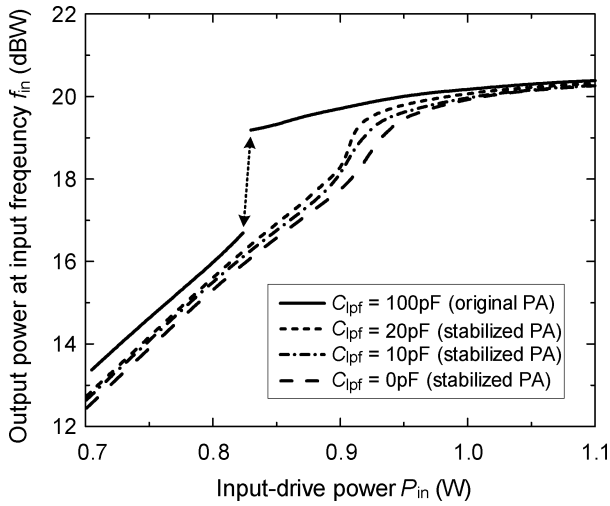

Fig. 10. Measured $P_{\rm in} - P_{\rm out}$ transfer characteristics before and after the elimination of the hysteresis. For the stabilized PA, only the curves without oscillation are presented.

was suppressed for a capacitor value smaller than 30 pF. Although this value is lower than the one obtained in simulation (50 pF), there is a good qualitative agreement with the predictions of Fig. 9. The reduction of $C_{\rm lpf}$ value eliminates the hysteresis with minimum disturbance of the power-transfer curve. As the capacitor value decreases, the intermediate range of the curve becomes smoother and shifts to the right in similar manner to Fig. 9.

For a chosen capacitor value $C_{\rm lpf} = 20$ pF, all the output harmonic levels were suppressed more than 50 dB below the fundamental so the low-pass filter still fulfills the original purpose. No oscillation was observed when varying the input power, but the bumps were still noticeable in the spectrum, both corresponding to the simulations. Thus, an additional technique is needed for the elimination of the noisy precursors. This will be presented in Section VI.

VI. Elimination of Noisy Precursors

From the analysis of Section IV, the precursors of the Class-E amplifier are due to the proximity of the pair of poles $\sigma_1 \pm j2\pi f_1$ to the imaginary axis with $\sigma_1 < 0$ for all the $P_{\rm in}$ values. According to (1), for a reduction of the precursor power, we need to move σ_1 away from the axis. A possible technique is the parallel connection of a resistance to the transistor drain terminal. This will increase the real part of the input admittance looking from the drain terminal at f_1, and move the near-critical poles $\sigma_1 \pm j2\pi f_1$ leftward, which will give rise to the increase of the stability margin.

On the other hand, the resistance at the transistor output will substantially degrade the drain efficiency and output power of the amplifier. To avoid this degradation, an inductor of relatively high value is connected in series with the resistor. Thus, the correction network is composed of a stabilization resistance of 33 Ω, an inductor of 4 μH, and a dc-blocking capacitor of 80 nF in series. This network is connected in parallel at the drain terminal. With the addition of the inductor, the impedance exhibited at $f_{\rm in}$ will be large, and little current will flow at that frequency.

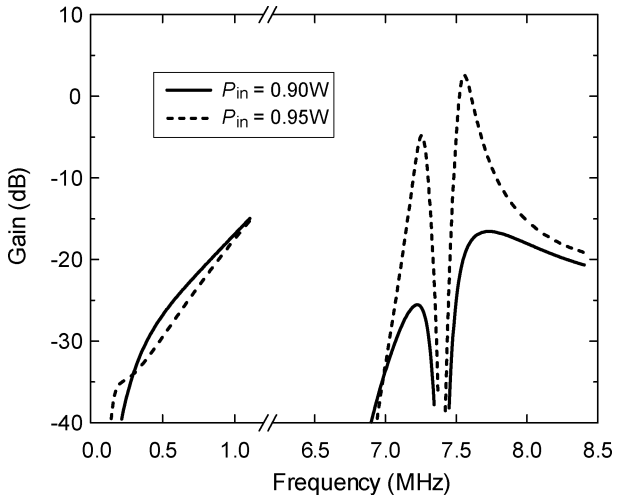

Fig. 11. Corrected amplifier. Frequency variation of the current gain from the channel-noise current source to the circuit output, calculated with the conversion matrix approach.

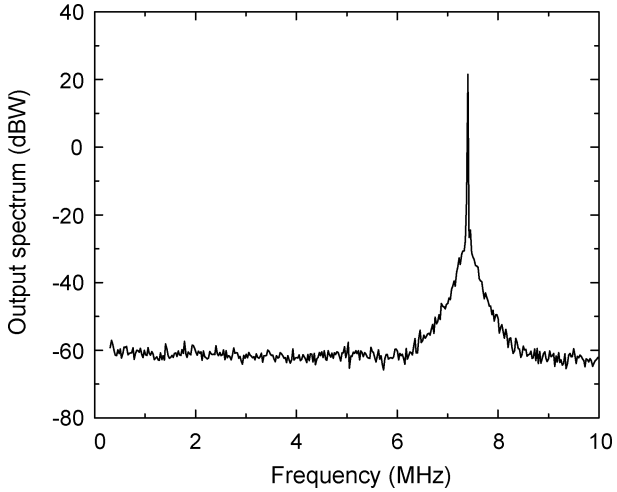

Fig. 12. Measured output power spectrum of the corrected amplifier at $P_{\rm in} = 0.95$ W. The noise from the input-drive source is still present about $f_{\rm in}$. However, the noise bumps have disappeared, which validates the proposed correction technique.

Due to the fact that the resonance frequency f_c is relatively close to $f_{\rm in}$, the impedance of the inductor at f_c will affect the system poles. To analyze this influence, the pole locus versus $P_{\rm in}$ has been retraced. The introduction of the inductance removes the former complex-conjugate poles $\sigma_1 \pm j2\pi f_1$. Instead, it creates a new pole pair $\sigma_1' \pm j2\pi f_1'$ also close to the imaginary axis, with f_1' being significantly smaller than f_1 for the entire $P_{\rm in}$ range. However, the observation of the precursors is also strongly dependent on the gain from the noise sources to the amplifier output at the near-critical frequencies $f_1', f_{\rm in} - f_1', f_{\rm in} + f_1', \ldots$. This gain has also been analyzed with the results of Fig. 11. Compared with Fig. 6, there is a substantial gain decrease for all the $P_{\rm in}$ values. This is due to high attenuation of the embedding circuit at the much lower value f_1' of the near-critical frequency. The gain curves about the input-drive frequency maintain the Lorentzian shape. Similar low-gain values are obtained when sweeping the current source about $f_{\rm in} - f_1'$ or $f_{\rm in} + f_1'$.

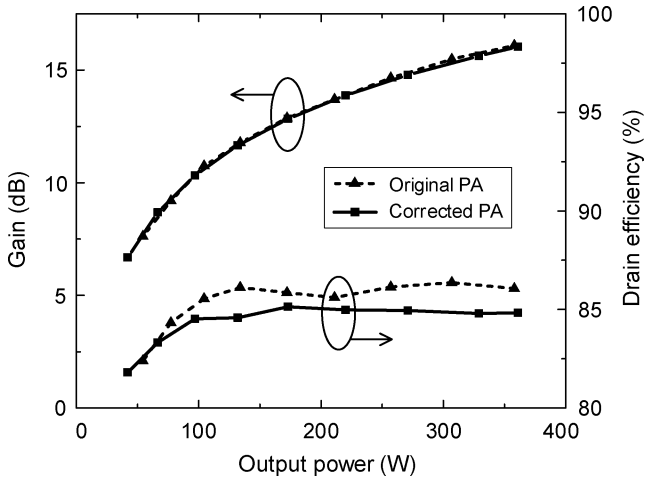

Fig. 13. Comparison of the measured gain and drain efficiency versus the output power between the original and corrected amplifiers. The input power is 9 W for saturated switching operation in the entire measurements.

The elimination of the precursors has been experimentally confirmed. No precursors or instability were obtained in the measurements for the entire range of input power and drain bias voltage, which is in agreement with the simulations. Fig. 12 shows a representative measurement of the output power spectrum corresponding to $P_{\rm in} = 0.95$ W. The noise coming from the input-drive source is still present about $f_{\rm in}$, but unlike the spectrum of Fig. 2(b), no noise bumps are observed about $f_{\rm in}$ or at low frequency. The measured gain and drain efficiency of the corrected amplifier is shown in Fig. 13. Compared with the original amplifier, the degradation of the drain efficiency is below 1.5% for all output power levels. The gain is almost same because of the saturated switching operation of the amplifier.

VII. Conclusion

In this study, techniques have been presented for the in-depth analysis of complex instability phenomena in PAs. They have enabled the understanding of the anomalous behavior of a Class-E PA, involving hysteresis in the $P_{\rm in} - P_{\rm out}$ curve, noisy precursors, self-oscillation, and harmonic synchronization. A general technique has been provided for the efficient elimination of hysteresis in the $P_{\rm in} - P_{\rm out}$ curve of PAs. It is based on the tracing of a turning point locus in the plane defined by the input power and one stabilization parameter. The technique has been applied to the Class-E amplifier with good results. The noisy precursors have also been analyzed and the circuit characteristics that determine their practical observation have been investigated. A technique has been presented for their efficient elimination from the output power spectrum, which has been successfully applied to the Class-E PA.

Acknowledgment

The authors would like to thank C. Wheatley, Qualcomm, San Diego, CA, for support. The authors would also like to thank J.-M. Collantes, University of the Basque Country, Bilbao, Spain, for helpful comments.

REFERENCES

[1] D. Teeter, A. Platzker, and R. Bourque, "A compact network for eliminating parametric oscillations in high power MMIC amplifiers," in *IEEE MTT-S Int. Microw. Symp. Dig.*, Anaheim, CA, Jun. 1999, pp. 967–970.

[2] A. Collado, F. Ramírez, and A. Suárez, "Analysis and stabilization tools for microwave amplifiers," in *IEEE MTT-S Int. Microw. Symp. Dig.*, Fort Worth, TX, Jun. 2004, pp. 945–948.

[3] M. Mochizuki, M. Nakayama, Y. Tarui, Y. Itoh, S. Tsuji, and T. Takagi, "Nonlinear analysis of $f_o/2$ loop oscillation of high power amplifiers," in *IEEE MTT-S Int. Microw. Symp. Dig.*, Orlando, FL, May 1995, pp. 709–712.

[4] S. Jeon, A. Suárez, and D. B. Rutledge, "Global stability analysis and stabilization of a class-E/F amplifier," *IEEE Trans. Microw. Theory Tech.*, vol. 53, no. 12, pp. 3712–3722, Dec. 2005.

[5] S. Mons, J.-C. Nallatamby, R. Queré, P. Savary, and J. Obregon, "A unified approach for the linear and nonlinear stability analysis of microwave circuits using commercially available tools," *IEEE Trans. Microw. Theory Tech.*, vol. 47, no. 12, pp. 2403–2409, Dec. 1999.

[6] J. Jugo, J. Portilla, A. Anakabe, A. Suárez, and J. M. Collantes, "Closed-loop stability analysis of microwave amplifiers," *Electron. Lett.*, vol. 37, pp. 226–228, Feb. 2001.

[7] A. Anakabe, J. M. Collantes, J. Portilla, J. Jugo, S. Mons, A. Mallet, and L. Lapierre, "Analysis of odd-mode parametric oscillations in HBT multi-stage power amplifiers," in *Eur. Microw. 11th GaAs Symp.*, Munich, Germany, Oct. 2003, pp. 533–536.

[8] E. Lau, K.-W. Chiu, J. Qin, J. Davis, K. Potter, and D. Rutledge, "High-efficiency class-E power amplifiers—Part 1," *QST*, pp. 39–42, May 1997.

[9] C. Jeffries and K. Wiesenfeld, "Observation of noisy precursors of dynamical instabilities," *Phys. Rev. A, Gen. Phys.*, vol. 31, no. 2, pp. 1077–1084, Feb. 1985.

[10] S. Ver Hoeye, A. Suárez, and S. Sancho, "Analysis of noise effects on the nonlinear dynamics of synchronized oscillators," *IEEE Microw. Wireless Compon. Lett.*, vol. 11, no. 9, pp. 376–378, Sep. 2001.

[11] A. Suárez and R. Queré, *Global Stability Analysis of Microwave Circuits*. Boston, MA: Artech House, 2003.

[12] V. Rizzoli and A. Neri, "State of the art and present trends in nonlinear microwave CAD techniques," *IEEE Trans. Microw. Theory Tech.*, vol. 36, no. 12, pp. 343–365, Feb. 1988.

[13] L. O. Chua, "A switching-parameter algorithm for finding multiple solutions of nonlinear resistive circuits," *Int. J. Circuit Theory Applicat.*, vol. 4, no. 3, pp. 215–239, Jul. 1976.

[14] V. Rizzoli, F. Mastri, and D. Masotti, "General noise analysis of nonlinear microwave circuits by the piecewise harmonic-balance technique," *IEEE Trans. Microw. Theory Tech.*, vol. 42, no. 5, pp. 807–819, May 1994.

[15] E. Ngoya and R. Larcheveque, "Envelope transient analysis: A new method for the transient and steady state analysis of microwave communication circuits and systems," in *IEEE MTT-S Int. Microw. Symp. Dig.*, San Francisco, CA, Jun. 1996, pp. 1365–1368.

[16] J. C. Pedro and N. B. Carvalho, "Simulation of RF circuits driven by modulated signals without bandwidth constraints," in *IEEE MTT-S Int. Microw. Symp. Dig.*, Seattle, WA, Jun. 2002, pp. 2173–2176.

[17] N. O. Sokal and A. D. Sokal, "Class E—A new class of high-efficiency tuned single-ended switching power amplifiers," *IEEE J. Solid-State Circuits*, vol. 10, no. 3, pp. 168–176, Jun. 1975.

[18] M. Albulet, *RF Power Amplifiers*. New York: Noble, 2001.

[19] J. M. T. Thompson and H. B. Stewart, *Nonlinear Dynamics and Chaos*. New York: Wiley, 1986.

[20] F. Ramirez, M. E. de Cos, and A. Suárez, "Nonlinear analysis tools for the optimized design of harmonic-injection dividers," *IEEE Trans. Microw. Theory Tech.*, vol. 51, no. 6, pp. 1752–1762, Jun. 2003.

[21] F. X. Kaertner, "Analysis of white and f^{α} noise in oscillators," *Int. J. Circuit Theory Applicat.*, vol. 18, pp. 485–519, 1990.

[22] R. E. Collin, *Foundations for Microwave Engineering*, 2nd ed. New York: IEEE Press, 2001.

[23] K. Kurokawa, "Some basic characteristics of broad-band negative resistance oscillator circuits," *Bell Syst. Tech. J.*, vol. 48, pp. 1937–1955, Jul.–Aug. 1969.

[24] J. Guckenheimer and P. Holmes, *Nonlinear Oscillations, Dynamical Systems and Bifurcations of Vector Fields*. Berlin, Germany: Springer-Verlag, 1990 (third printing).

Sanggeun Jeon (S'05) received the B.S. and M.S. degrees in electrical engineering from Seoul National University, Seoul, Korea, in 1997 and 1999, respectively, the M.S. degree in electrical engineering from the California Institute of Technology, Pasadena, in 2004, and is currently working toward the Ph.D. degree at the California Institute of Technology.

From 1999 to 2002, he was a Full-Time Instructor of electronics engineering with the Korea Air Force Academy, Cheongwon, Korea. His research interests include high-efficiency PAs and nonlinear stability analysis.

Mr. Jeon was the recipient of the Third Place Award in the Student Paper Competition at the 2005 IEEE Microwave Theory and Techniques Society (IEEE MTT-S) International Microwave Symposium (IMS).

Almudena Suárez (M'96–SM'01) was born in Santander, Spain. She received the Electronic Physics and Ph.D. degrees from the University of Cantabria, Santander, Spain, in 1987 and 1992, respectively, and the Ph.D. degree in electronics from the University of Limoges, Limoges, France, in 1993.

In 1987, she joined the Electronics Department, University of Cantabria, where she was involved with nonlinear simulation. From May 1990 to December 1992, she was on leave with the Institute de Recherche en Communications Optiques et Microondes (IRCOM), University of Limoges. Since 1993, she has been an Associate Professor (permanent since June 1995) with the Communications Engineering Department, University of Cantabria. She coauthored *Stability Analysis of Microwave Circuits* (Artech House, 2003). Her areas of interest include the nonlinear design of microwave circuits, especially the nonlinear stability and phase-noise analysis and the investigation of chaotic regimes.

David B. Rutledge (S'77–M'77–SM'89–F'93) received the B.A. degree in mathematics from Williams College, Williamstown, MA, the M.A. degree in electrical sciences from Cambridge University, Cambridge, U.K., and the Ph.D. degree in electrical engineering from the University of California at Berkeley.

He is currently the Tomiyasu Professor of Electrical Engineering with the California Institute of Technology, Pasadena. He is Director of the California Institute of Technology's Lee Center for Advanced Networking. He authored the electronics textbook *The Electronics of Radio* (Cambridge Univ. Press, 1999) and coauthored the microwave computer-aided-design software package *Puff*, which has sold 30 000 copies. His research has been in integrated-circuit antennas, active quasi-optics, computer-aided design, and high-efficiency PAs.

Prof. Rutledge was the recipient of the Microwave Prize, the Distinguished Educator Award of the IEEE Microwave Theory and Techniques Society (IEEE MTT-S), the Teaching Award of the Associated Students of the California Institute of Technology, the Doug DeMaw Award of the American Radio Relay League (ARRL), and the Third Millennium Award of the IEEE. He was the editor-in-chief of the IEEE TRANSACTIONS ON MICROWAVE THEORY AND TECHNIQUES, and a Distinguished Lecturer of the IEEE Antennas and Propagation Society (IEEE AP-S).